43. Glasses for Photonic Integration

Inorganic glasses are the workhorse materials of optics and photonics. In addition to offering a range of transparency windows, glasses provide flexibility of processing for the realization of fibers, films, and shaped optical elements. Traditionally, the main role of glass has been as a passive material. However, a significant attribute of glasses is their ability to incorporate dopants such as nanoparticles or active ions. Hence, glasses promise to play an increasingly important role in active photonics, as laser, amplification, switching, and nonlinear media.

For photonic integration, many of the attributes of glasses are particularly compelling. Glasses allow numerous options for thin film deposition and integration on arbitrary platforms. The possibility of controlling the viscosity of a glass during processing can be exploited in the realization of extremely low loss microphotonic waveguides, photonic crystals, and microcavities. The metastable nature of glass can enable the direct patterning of photonic elements by energetic beams.

This chapter provides an overview of these unique properties of glasses, from the perspectives of the technology options they afford and the practical limitations they present. Further, an overview is provided of the main families of glassy inorganic films studied for integrated optics. Finally, the main features of rare earth doped glasses are reviewed, with an emphasis on their potential for implemention of compact integrated light sources and amplifiers.

Inorganic glasses have played a central role in optical science and technology, and more generally within the electrical and electronic engineering disciplines [43.1]. Amongst optical materials, the unique advantages of glasses are well known [43.2, 3]. Glasses can be worked relatively easily into various forms, such as bulk lenses, fibers, and thin films. This is dramatically illustrated by the modern technology for the manufacture of low-loss silica fibers, in which a hair-thin glass fiber (with tightly controlled geometrical and material properties) is drawn from a heated glass preform at rates as high as 20 m/s or greater [43.4]. Glass can be manufactured with excellent homogeneity and without grain boundaries, so that scattering of light is acceptably low. While perfect crystals typically exhibit even lower levels of scattering, they are difficult to realize in large sizes and with arbitrary shapes. Optical losses in polycrystalline materials, on the other hand, are generally excessive due to scattering from grain boundaries. Finally, the standard glass compositions (oxide, halide, and chalcogenide glasses and hybrids of those) provide transparency windows from the UV to the mid-infrared (see Fig. 43.1). It has been estimated [43.2] that more than 90% of optical components are based on glasses. Given the massive worldwide installation of telecommunications fibers since the 1980s [43.5], and depending on the definition assigned to the term 'component', this statistic might actually be closer to 100%.

Befitting their central role in optical technology, there are numerous excellent reviews covering

the optical properties and photonic functionalities of glasses [43.3, 6]. Further, one of the distinguishing attributes of glasses is their flexibility of composition. Hundreds of commercial glasses are available, and many more have been studied in research laboratories and reported in the academic literature. Thus, it is not possible to capture the full range of glassy materials (even restricted to inorganic glasses) within a short review paper. The recent monograph by *Yamane* and *Asahara* [43.6] provides a comprehensive and highly recommended treatment of glass technology and its application to photonics. The present contribution has relatively modest aims:

1. With a focus specifically on *integrated* photonics, the main advantages of glasses are discussed and the most studied glass systems are reviewed in brief. Integrated photonics (integrated optics) refers to guided wave photonic devices fabricated on planar platforms. Glass substrates (with waveguides defined by ion diffusion) have played an important role in integrated optics, but the advantages of glasses (compared to crystalline materials such as III-V semiconductors or lithium niobate) are less compelling in that case. For this reason, emphasis is placed on glassy thin films that can enable photonic functionality on other substrates. In practice, substrates of interest might be printed circuit boards or semiconductor wafers.
2. For the most part, the discussion is restricted to inorganic glasses. Some reference is made to organic glasses, since their properties and advantages parallel those of inorganic glasses in many respects, and because certain practical aspects of organic glasses have received greater attention in the literature. Good reviews covering polymer materials for integrated photonics are available [43.8].
3. To date, the most important inorganic glass system for integrated photonics is the silica on silicon planar lightwave circuit (PLC) platform. Several recent papers [43.9, 10] provide an overview of that technology, so only brief mention is made here. Rather, the goal is to provide some insight on advantages that are globally associated with glassy materials. Further, an emphasis is placed on the unique advantages (lower processing temperatures, higher refractive index contrast, active functionality, etc.) enabled by some glass systems.

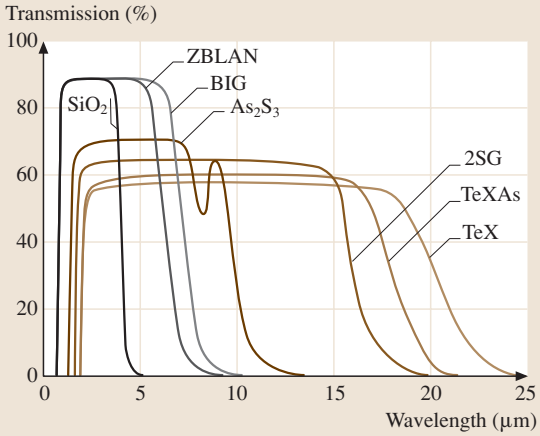

Fig. 43.1 Transmission plots are shown for SiO_2 glass and some representative fluoride and chalcogenide glasses. ZBLAN and BIG are heavy-metal fluoride glasses, 2SG is a selenide glass, and TeXAs and TeX are tellurium-based chalcogenide glasses. (After [43.7])

With these goals in mind, the chapter is organized as follows. In Sect. 43.1, we highlight the main advantages of glasses for photonic integration. These attributes include the unique processing options afforded by the existence of the glass transition and by the metastability of glasses. Section 43.2 provides an overview of the most-studied materials for glass-based integrated optics. This includes the standard glass formers (oxide, halide, chalcogenide glasses) as well as several materials that are generally classified as ceramics (Si_3N_4, Al_2O_3, etc.) but which can be realized as amorphous thin films. In Sect. 43.3, some unique advantages of glasses for realization of integrated light sources are reviewed. Section 43.4 provides a summary and some thoughts on future prospects for glasses in photonic integration.

43.1 Main Attributes of Glasses as Photonic Materials

The essential characteristic of a glass is the existence of a glass transition temperature (T_g). In short, if a viscous liquid is cooled fast enough, the liquid passes through the freezing temperature of the material without making a phase transition to the solid crystalline state (see Fig. 43.2). Rather, it becomes a supercooled liquid, whose rate of change of specific volume (or enthalpy) with decreasing temperature remains constant

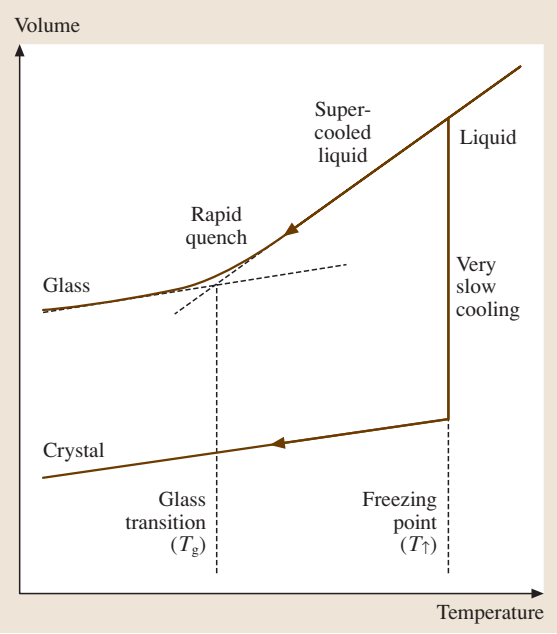

Fig. 43.2 Schematic plot illustrating the change in specific volume of a glass with temperature (after [43.11])

and equivalent to that of the molten liquid. At T_g, the slope of these curves (for example, specific volume versus temperature) changes abruptly (but in a continuous way) to a value that is approximately that of the corresponding crystal. Below T_g, the material is an amorphous solid or glass.

While glass forming has been a staple of human technological innovation for thousands of years, the physical processes underlying the glass transition are still a matter of some debate [43.11–13]. Several empirical facts are well known, however. The glass transition temperature of a particular material is not a constant, but is somewhat dependent on processing details such as the rate of cooling from the melt, or more generally on the technique used to form the glass (melt quenching, thin film deposition, etc.) and even the age of the glass [43.14]. T_g is slightly higher for a faster rate of cooling from a melt, for example, but in general $T_g \approx 2T_m/3$, where T_m is the melting/freezing temperature of the material [43.12]. For glasses that cannot be formed easily by melt quenching, such as amorphous Si [43.13], the direct experimental determination of T_g is not always possible, and indirect methods are sometimes used to estimate an effective T_g.

Central to the technological application of glasses is the ability to control their viscosity by way of temperature [43.5]. For stable glass formers, it is possible to transition between states of very low viscosity (molten liquid), low viscosity (supercooled liquid), and high viscosity (frozen liquid; i. e. glass). This remarkable variation in mechanical properties with temperature, spanning several orders of magnitude in viscosity, underpins both the ancient and modern manufacture of glass products (by molding, extrusion, float processes, etc.). It is interesting to note that T_g can be defined as the approximate temperature at which the shear viscosity attains 10^{12} Pa s. Further, viscosity varies rapidly in the vicinity of T_g. For so-called strong glass formers (such as SiO_2), the viscosity η varies according to an Arrhenius equation of the form $\eta = A \exp(B/k_B T)$, where A and B are temperature-independent constants and k_B is the Boltzmann constant [43.12]. To form glasses into desired shapes, the temperature is typically controlled such that the viscosity is in the 10^2 to 10^7 Pas range, depending on the process and the stability of the particular glass composition [43.6, 15].

It was once held that only certain materials could form glasses, but it is now believed that the glassy state is attainable for all types of materials [43.11]. Accordingly, the literature contains references to various families of glasses, including inorganic (ceramic), organic (polymeric), and metallic glasses.

43.1.1 The Glass Transition as Enabler

The surface tension of liquids is a well-known enabler of optical quality surfaces [43.16]. Glass devices can be formed in the liquid state, and can thus accommodate manufacturing processes that are assisted by surface tension mediated self-assembly. The manufacture of modern single mode fibers is a good example of the enabling nature of the glass transition. In a typical process [43.4, 6, 17], highly purified glass layers are deposited either on the inside walls of a fused silica tube by chemical vapor deposition (CVD) or on the outside surface of a ceramic rod by flame hydrolysis deposition (FHD). The hollow glass cylinder (after removal of the ceramic rod in the latter case) is then heated (sintered) to $\approx 1600\,^\circ$C, such that it collapses to form a solid glass preform (typically 1 m in length and 2 cm in diameter). 1600 °C is the approximate softening point of silica glass, typically defined as corresponding to a viscosity of $\approx 10^7$ Pas [43.6]. The fiber drawing process involves local heating of the preform to a temperature of approximately 2000 °C (corresponding to a viscosity of $\approx 10^5$ Pa s). Thus, viscosity control is critical at nearly all stages of the process. Further, the drawing process allows tremendous control over the optical and

geometrical properties of the fiber, in part due to the self-regulating properties of surface tension effects in the supercooled liquid. As an added benefit, inhomogeneities in the original preform tend to be averaged out in the process [43.18]. The amazing properties of silica fibers (tensile strength comparable to that of steel, low loss, and extremely tight tolerances for material and geometrical parameters) are well known, and attest to the technological versatility of (silica) glasses. It is also interesting to note that the standard technique for splicing sections of silica fibers together, which is achieved with less than 0.1 dB loss [43.5], is based on a reflow process wherein surface tension contributes to their alignment.

Within integrated optics, the manufacture and optimization of PLC devices relies directly on the glass transition in many cases [43.9, 10]. PLC devices are manufactured in doped SiO_2 glasses deposited (by CVD, FHD, or sol-gel techniques) on a silicon wafer. The undercladding is often pure SiO_2, which can be formed by thermal oxidation of the silicon wafer. Typically, dopants in the core and uppercladding layers act to modify both the refractive index and the thermo-mechanical properties of the glass. In particular, controlled reflow (by heating the glasses near T_g) of these layers often plays an important part in the process. Reflow is used to consolidate the interface between layers, to smoothen the rough sidewalls of the waveguide core (formed by dry etching processes), and to assist in gap filling and planarization of the cladding layer over the patterned core layer [43.9], [43.18–20]. Typically, the layers are doped such that the glass transition decreases in the upward direction. In that way, a layer can be reflowed without affecting the underlying layers. As an example, a 'pinned based reflow' is shown in Fig. 43.3 [43.19]. The circle-section shaped core arises from selective reflow of the core material while its interface with the undercladding glass remains fixed. The upper boundary of the core is shaped by surface tension.

Surface tension driven manufacture of more exotic optical components has been widely studied. Examples include silica-glass based optical microcavities [43.21–23], nm-scale silica wires [43.24], photonic crystal fibers [43.25], microball lenses [43.26], and microlenses [43.27, 28]. In these cases, the reduction of scattering losses by surface tension mediated smoothening of interfaces is particularly important.

As discussed further in Sect. 43.2, high index contrast waveguides, photonic crystals, and microcavities are major themes within integrated optics. High index contrast (between the core and cladding of a waveguide, for example) is desirable because it enables strong confinement of light to small waveguides or small resonant cavities. This is essential to the realization of high-density integrated optics [43.9]. The downside of high index contrast is that scattering at interfaces increases with index contrast. This is clarified by the so-called Tien model for waveguide loss due to interfacial scattering in a symmetric slab waveguide [43.29]:

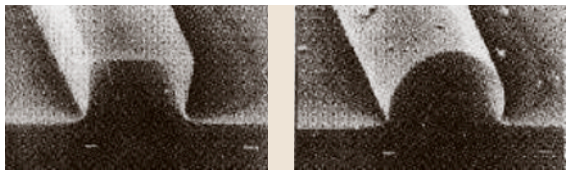

Fig. 43.3 A glass waveguide core is shown before (*left*) and after (*right*) a selective reflow process (From [43.19]

$$\alpha_S = \frac{2\sigma^2 k_0^2 h}{\beta}\Delta n^2 E_S^2 \qquad (43.1)$$

where σ is the standard deviation (characteristic amplitude) of the roughness, k_0 is the free-space wavenumber, h is the inverse of the penetration depth of the mode into the cladding, β is the propagation constant of the mode, and E_S is the normalized electric field amplitude at the core-cladding interface. Further, $\Delta n^2 = n_{\text{core}}^2 - n_{\text{clad}}^2$, where n_{core} and n_{clad} are the core and cladding refractive indices, respectively. This equation explicitly shows the strong dependence of scattering loss on index contrast. A more accurate expression, derived by considering the statistics of roughness (not just the amplitude), is the Payne-Lacey model [43.30]:

$$\alpha_S = 4.34\frac{\sigma^2}{k_0\sqrt{2}d^4 n_{\text{core}}}\cdot g \cdot f \qquad (43.2)$$

where d is the core thickness, g is a function that depends mainly on the core-cladding index offset, and f is a function that depends on the statistics of the roughness. If $r(z)$ is the random function describing the line-edge roughness (i. e. the deviation of the core-cladding interface from a straight line), the autocorrelation of $r(z)$ is often well described by an exponential function [43.31]:

$$R(u) = \langle r(z)r(z+u)\rangle \approx \sigma^2 \exp\left(\frac{-|u|}{L_c}\right) \qquad (43.3)$$

where L_c is the so-called correlation length. It can be shown that for waveguide geometries of typical interest, low scattering loss requires both σ and L_c to be low. As a second illustration of the impact of interface roughness, it can be shown that the surface scattering limited quality (Q) factor for whispering gallery modes in a spherical

microsphere is approximately [43.23]:

$$Q_{SS} = \frac{\lambda^2 D}{2\pi^2 \sigma^2 L_c} \tag{43.4}$$

where D is the microsphere diameter. Again, minimization of scattering losses is correlated with minimization of σ and L_c.

It is interesting to compare recent results for high index contrast structures in crystalline materials and glasses. Much of the work on very highly confining waveguides and photonic crystals has focused on semiconductor material systems, especially the silicon-on-insulator (SOI) system [43.29, 30] and III-V semiconductor systems [43.33]. Generally, structures are defined by electron-beam or photolithography, followed by a dry etching process. Each of these steps has limited precision and contributes to the overall roughness [43.31]. With use of sophisticated processes, roughness parameters are typically on the order of $\sigma \approx 5$ nm and $L_c \approx 50$ nm, resulting in losses on the order of 3–10 dB/cm for sub-micron strip waveguides [43.30]. Significant improvement in these numbers is mostly reliant on advancements in lithography or etching processes. These same issues limit the performance of other high index contrast structures formed in semiconductors. For example the Q factor of semiconductor microdisk and microring resonators typically does not exceed 10^5 [43.34], and the loss of photonic crystal defect waveguides in semiconductors remains impractically large [43.35].

By comparison, glasses (at least certain glasses) offer the potential for much smaller characteristic roughness. If a glass is formed from a supercooled liquid state, surface tension effects can produce glass surfaces with nearly atomic level smoothness. The roughness of a melt-formed or reflowed glass surface is determined by surface capillary waves, which are small amplitude fluctuations at a liquid surface that become frozen in place at T_g [43.25]. The resulting RMS roughness is approximately given by [43.36]:

$$\sigma \approx \sqrt{\frac{k_B T_g}{\gamma(T_g)}} \tag{43.5}$$

where $\gamma(T_g)$ is the surface tension of the supercooled liquid at T_g. For silica glass, this equation predicts rms roughness on the order of 0.1 nm or less, and the correlation length of this inherent roughness is estimated to be as small as 3 nm [43.23]. Note that glasses with lower T_g and/or higher surface tension can in theory exhibit even lower values of surface roughness. Interestingly, sub-nm surface roughness has been experimentally verified

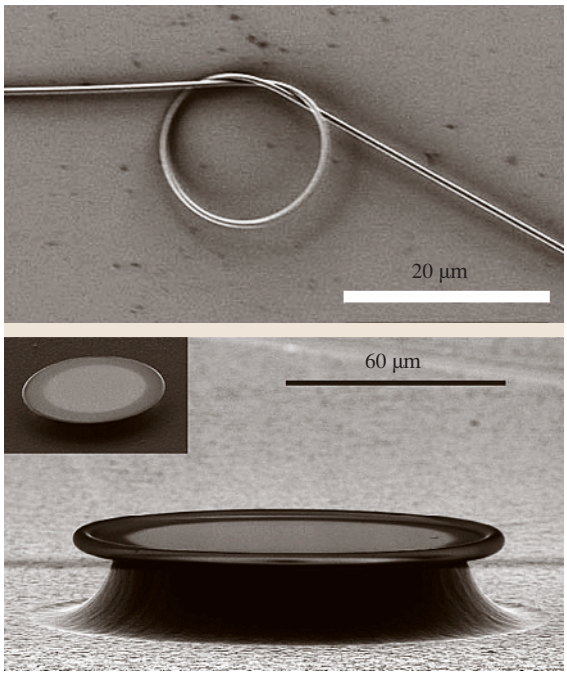

Fig. 43.4 **(a)** A submicron silica glass wire with sub-nm surface roughness is shown [43.24]. **(b)** A silica glass toroid sitting atop a silicon post is shown. The atomic-level smoothness of the toroid surface was achieved using a selective reflow process. (After [43.32])

for both melt-formed and fractured surfaces of silica glass [43.36] and indirectly from loss measurements in photonic crystal fibers [43.25]. Sub-nm roughness has also been determined for wet-etched surfaces of SiO_2 glass [43.37] and is not untypical for glass films deposited by evaporation.

The smoothness of glass surfaces has important implications for realization of low loss microphotonic devices, as evidenced by several recently reported results. While little work has been conducted on small core, high index contrast planar waveguides in glass, a method for fabricating sub-micron silica wires was recently reported [43.24] (see Fig. 43.4a). The authors estimated the rms surface roughness of their wires to be less than 0.5 nm, and demonstrated losses on the order of 1 dB/cm at 633 nm for 400 nm diameter wires. Sub-nm surface roughness has also been measured in the case of sol-gel glass microlenses formed by a reflow process [43.27]. Silica glass based microsphere cavities, typically formed by melting the end of fused silica fiber, exhibit Q factors of nearly 10^{10} [43.22, 23], the highest for any solid state microcavity. Recently, this concept

has been extended [43.21, 32] to the manufacture of silica toroid microresonators on a silicon substrate (see Fig. 43.4b). The latter devices exhibit Q factors exceeding 10^8. Finally, glass-based photonic crystal fibers have been demonstrated to exhibit scattering loss near fundamental limits set by surface capillary waves [43.25]. This last result contrasts with the situation mentioned above for semiconductor photonic crystals, which to date are significantly compromised by optical scattering.

In summary, processing enabled by the glass transition clearly offers unique benefits for manufacture of microphotonic structures. It is necessary to add a caveat to this discussion, however. Many amorphous materials are conditional glass formers, and do not offer the full range of processing advantages outlined above. As an extreme example, amorphous silicon films typically crystallize at temperatures well below their effective glass transition temperature [43.13], and are not amenable to reflow processes. To varying degrees, this is true of many 'glassy' films used in integrated optics, such as silicon oxynitride and alumina. Further, the tendency towards crystallization varies greatly even amongst the traditional glass formers, as discussed below. Thus, chalcogenide and fluoride glasses will not generally support the range of viscosity control that enabled many of the SiO_2-based devices mentioned. Having said that, novel techniques can sometimes circumvent crystallization problems. For example, pressure can be used as a tool for forming glass devices at temperatures below the onset of severe crystallization (but high enough to enable the glass to flow). Chalcogenide glass based lenses molded by the application of pressure and temperature are now commercially available [43.38]. Another interesting example is the recent work on extruded channel waveguides reported by *Mairaj* et al. [43.39]. Finally, much research has been directed at the fabrication of microphotonic elements in organic glasses by hot embossing [43.8]. In this technique, a hard master (such as a silicon wafer) is pre-patterned with the negative image of the desired photonic circuitry. The glass is heated above T_g and the master is pressed against the glass such that the image of its pattern is transferred to the softened glass. While studied mainly in polymer, this technique might also be applicable to low cost fabrication of photonic structures in 'soft' inorganic glasses.

43.1.2 Metastability

A glass is a metastable material, having been frozen as an amorphous solid possessing excess internal energy relative to the corresponding crystal. Metastability is a double-edged sword. On the one hand, it presents technological limitations with respect to the processing and use of a glass device. As an example, it is well known that commercial introduction of organic glass (polymer) based optical devices has been hindered by poor stability of many polymers at elevated temperatures or under exposure to high intensity light. On the other hand, metastability offers unique options for fabrication and optimization of photonic microstructures. Specifically, glass properties (optical, mechanical, chemical) can often be tailored or adjusted by the careful addition of energy, in the form of heat, light, electron beams, or ion beams. An example is provided by the commercially important fiber Bragg gratings (FBG), wherein UV light is used to induce a stable refractive index change in the Ge-doped core of a standard SiO_2-based fiber. In the following subsections, the implications of metastability for glass-based integrated photonics are discussed.

Devitrification

Well below its glass transition temperature, a glass sits in a local energy minimum and is impeded by its own viscosity from reaching the lower energy crystalline state. A frequently cited example is that of silicate glass windows in ancient buildings, which have not exhibited any significant crystallization. However, addition of sufficient energy (such as heating a glass to some temperature above T_g) can result in crystallization of a glass. Controlled crystallization is a technologically useful means of modifying the mechanical, thermal, or optical properties of a glass, used in the production of glass-ceramics. However, devitrification produces a polycrystalline material, increases optical scattering loss, and is usually a problem to be avoided in manufacture of photonic devices.

As mentioned in Sect. 43.1.1, crystallization tendencies vary widely between various glass systems. The difference between the onset temperature for crystallization and T_g, $\Delta T = T_x - T_g$, is one of the parameters that define the stability of a particular glass. The high stability against devitrification of silicate glasses is one of numerous reasons that they have traditionally dominated glass technology. This stability underlies the manufacture of the structures discussed in Sect. 43.1.1. Other glass forming systems have lower stability against devitrification, often making their technological application a greater challenge [43.39, 40]. For example, a major research thrust in the field of fluoride and chalcogenide glass fibers is the identification of new compositions that

exhibit improved stability against crystallization during the fiber drawing process [43.41].

For integrated optics, this form of stability is not always so critical. Amorphous thin films created by chemical vapor deposition, sputtering, evaporation, etc. can often be processed at temperatures below the onset of any significant crystallization. This enables the use of conditional glass formers, such as Si_3N_4, Al_2O_3 and semiconductors, in their amorphous state. However, it is interesting to review the early development of integrated optics, much of it focused on the identification of suitable thin film materials. Studies [43.43–45] that compared waveguide fabrication in polycrystalline (ZnO, ZnS, Al_2O_3, etc.) and amorphous (Ta_2O_5, polymer, sputtered glass) thin films showed that losses were orders of magnitude higher for the polycrystalline films. The lowest losses were initially obtained for polymer films [43.44], attributed to their amorphous structure and the smoothness of surfaces arising from spin casting of films.

If present, uncontrolled crystallization within films can be a dominant source of propagation loss [43.46]. For conditional glass formers, such as Al_2O_3 and TiO_2, crystallite formation must be carefully avoided during the deposition process [43.47]. While less of an issue for natural glass formers, the possibility for crystallization must always be considered when a glass film is subjected to high temperature processing steps.

Structural Relaxation

Having been frozen in some metastable configuration at the time of formation, an amorphous solid will always be subject to some degree of aging (changes in the material properties on some time scale). At temperatures below T_g, the glass is usually inhibited from crystallization by a significant internal energy barrier. However, subtler changes in the network structure can occur, such as the transition from the initial state to a more stable (but still amorphous) second state. This so-called structural relaxation is manifested in many ways – experiments often probe the change in time of specific volume, structural signatures (such as by Raman spectroscopy), or optical properties of the glass. The rate of structural relaxation is highly dependent on temperature, being relatively fast at temperatures near T_g and significantly slower for temperatures far below T_g [43.13]. In fact, annealing of glasses at a temperature near T_g is a standard technique used to promote rapid structural relaxation and lessen the dependence of material properties on the processing history [43.6]. In many cases, this annealing step is not practical, and structural relaxation over the in-use lifetime of a glass-based device must be considered.

As the following discussion will illustrate, the rate of structural relaxation at temperature T_1 exhibits a logarithmic dependence on the temperature difference $T_g - T_1$. Thus, T_g is an important parameter in character-

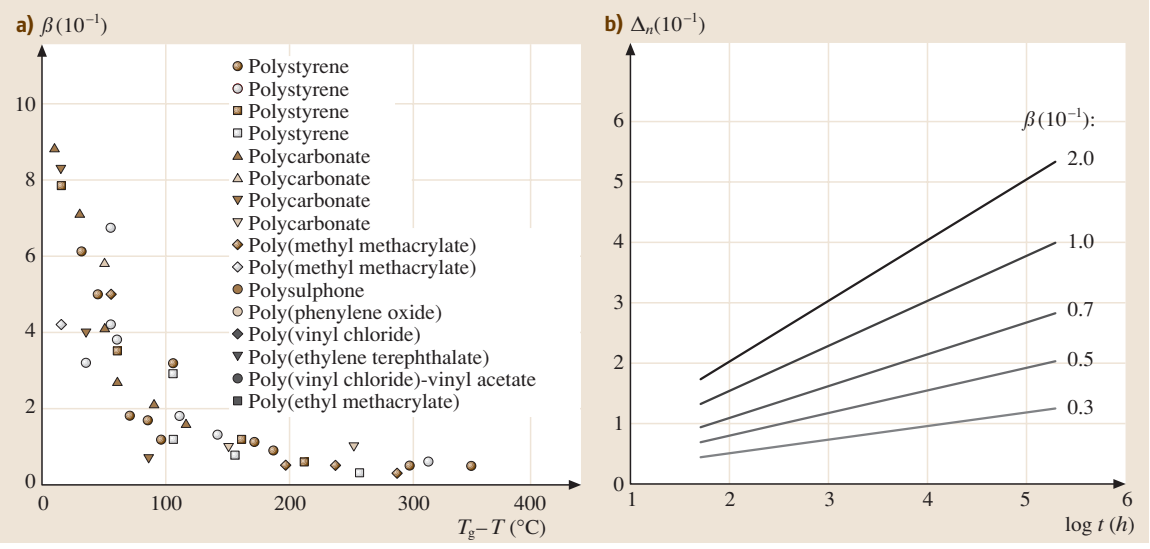

Fig. 43.5 **(a)** A plot of the structural relaxation rate parameter versus the supercooling temperature for a wide range of organic glasses is shown. **(b)** The predicted change in refractive index versus time for an organic glass, with the rate constant β as a parameter. (After [43.42])

izing the long-term stability of a glass component. For example, SiO_2 has a very high T_g ($\approx 1100\,^\circ C$) and does not exhibit significant relaxation at room temperature, either on the time scale of typical experiments or over the typical lifetimes envisioned for glass devices. In fact, aging effects in silica fibers are predominately associated with the growth of defects formed in the glass at the time of manufacture. Environmental moisture is a particular contributor to this aging process. On the other extreme, structural relaxation in low T_g organic glasses is known to be an issue, and intrinsic aging effects in polymers have been widely studied [43.48]. In particular, low T_g glasses exhibit densification with time (relaxation of their specific volume) and a corresponding change in their refractive index. This is a particular concern for interferometric optical devices (gratings, resonators, Mach–Zehnder interferometers), which necessitate tight control of material indices.

Volume relaxation can be characterized by a rate parameter β, defined as:

$$\beta = \frac{1}{V}\left[\frac{\partial V}{\partial (\log t)}\right]_{P,T} \tag{43.6}$$

where V is volume, t is time, P is pressure, and T is temperature. Using the Lorentz–Lorenz expression, the following relationship has been derived from (43.6) [43.42]:

$$\left[\frac{\partial n}{\partial (\log t)}\right]_{P,T} = \frac{-\beta\left(\frac{\partial n}{\partial T}\right)_{P,t}}{\alpha} \tag{43.7}$$

where n is refractive index, $\partial n/\partial T$ is the thermo-optic coefficient, and α is the volume coefficient of thermal expansion. *Zhang* et al. [43.42] further showed that, for polymers, β is approximately a universal function of $T_g - T_1$ as shown in Fig. 43.5. This implies that the time rate of change of refractive index due to structural relaxation is strongly correlated with the parameter $\Delta T_{SC} = T_g - T_1$, termed the supercooling temperature. They also assessed the implications for polymer-based telecommunications devices, concluding that T_g needs to be higher than 300 °C for many applications. This result provides a nice illustration of the impact of T_g on device stability.

While it is not necessarily reasonable to extend the foregoing results directly to inorganic glasses, the essential features of structural relaxation will be similar. The chalcogenide glasses in particular are sometimes called inorganic polymers, partly because of their softness and mechanical flexibility relative to silica-based glasses. Further, the range of T_g for chalcogenide glasses (≈ 50–$550\,^\circ C$) is similar to that of organic polymers, and studies on chalcogenide glasses [43.14] support the conclusion that structural relaxation would present similar restrictions on inorganic and organic glasses. Thus, lifetime restrictions due to relaxation should be considered in the application of any glass having relatively low T_g, including chalcogenide glasses, fluoride glasses, and many non-silicate oxide glasses [43.6].

Both the processing temperatures (during manufacture) and the in-use temperatures are important considerations in assessing the stability of a glass. Telecommunication devices are typically designed to withstand in-use temperatures between $-40\,^\circ C$ and $85\,^\circ C$ [43.49]. As an example of a more demanding application, it has been proposed that glasses are good candidates for fabrication of integrated photonic elements on future integrated circuit chips [43.50]. In-use temperatures on modern microprocessors can reach 100–200 °C.

Finally, it should be noted that any energy applied to the glass (light, electron beams, etc.) might induce structural relaxation. This has been most widely studied for the chalcogenide glasses, which exhibit a wide array of photoinduced structural changes [43.51]. A fascinating example is the so-called photoinduced fluidity phenomenon [43.52], in which intense sub-bandgap light can reduce the viscosity of a chalcogenide glass by several orders of magnitude (causing the glass to flow or melt). This effect is completely athermal, and in fact is often enhanced at low temperatures. While an extreme example, it illustrates the possibility of aging effects due to non-thermal processes in glass devices. For photonic devices, the main concern is usually the effect of light exposure over the in-use lifetime.

Metastability as Enabler

One highly desirable implication of metastability is the possibility for direct patterning of photonic structures in glasses using energetic beams (electron beams, ion beams, light). These effects can also be exploited for post-fabrication trimming of devices [43.53], which is important since many optical components have tolerances beyond the capabilities of practical fabrication processes.

Beam induced effects in glasses are generally linked to their random network structure. That is, unlike crystals, glasses contain a range of internal 'defects' – wrong bonds, dangling (missing) bonds, impurity atoms that act as network modifiers, as well as their inherent variation in bond angles. Addition of energy can cause a glass to undergo a transition from one metastable state to another. This transition is often accompanied by a change in the

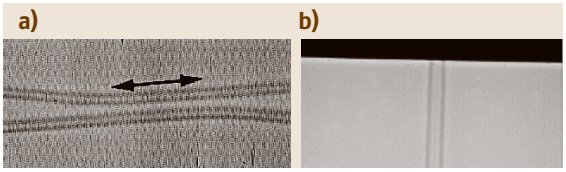

Fig. 43.6 **(a)** A directional coupler is shown, as written in a multicomponent silicate glass by an ultrafast Ti:sapphire laser [43.54]. The black arrow indicates the coupling region. **(b)** Microscope image of a rib waveguide formed by direct exposure of a chalcogenide glass (As_2Se_3) in a UV mask aligner, followed by wet etching [43.55]

density of defects or by a structural change – rearrangement or reorientation of bonds. Associated with these structural changes are changes in the physical, chemical, and optical properties of the glass. Most existing knowledge about these induced structural changes is of an empirical nature, whereas the underlying physical mechanisms are still the subject of research.

The ability to induce transitions between metastable states is probably a universal property of amorphous matter. Perhaps for practical reasons, such as the availability of light sources of suitable wavelength, metastability was initially studied in amorphous semiconductors and low band gap chalcogenide glasses. It should be added, though, that chalcogenide glasses seem to be unique with respect to the variety of induced structural changes they exhibit or at least the magnitude of those changes [43.51]. This might be related to the relatively weak, highly polarizable covalent bonds that are characteristic of chalcogenide glasses. Nevertheless, the later discovery [43.56] of photoinduced refractive index changes in Ge-doped silica glass prompted a huge research and development effort because of the technological importance of silicate glasses. The main outcome of this work was the fiber Bragg grating (FBG), which is a critical component in modern telecommunications and sensing networks. FBGs are manufactured by inducing a quasi-permanent index change within the Ge-doped core of a standard silica fiber, by exposure to an UV laser beam. Writing wavelengths are in the 150 to 350 nm range, corresponding to photon energies below the nominal bandgap of SiO_2. The mechanisms underlying the index increase are still debated [43.9, 56]. However, it is believed that contributing factors are absorption by defects in the glass (possibly generating further defects) and densification due to some sort of structural relaxation [43.57]. Typical index changes for standard fiber cores are in the 10^{-4} to 10^{-3} range, but several techniques (addition of other dopants, hydrogen-loading, etc.) have been developed to enable changes as high as 10^{-2}. Given the discussion in the preceding section, it is reasonable to ask whether photoinduced changes are themselves stable. The answer, in some cases, seems to be yes. Researchers have concluded that fiber Bragg gratings can have an operational lifetime of greater than 20 years, even at elevated temperatures of 80 °C [43.58].

Photosensitivity has been widely explored as a means to directly pattern integrated optics devices, especially in silica-based glasses [43.59]. In general, direct patterning is induced using photon energies close to the nominal bandgap energy of the glass or using intense light of lower photon energy [43.57]. In the latter case, photoinduced effects arise from nonlinear effects such as multi-photon absorption. In particular, the widely available Ti:sapphire laser has been applied to the writing of microstructures in a variety of glasses [43.54]. Because of the nonlinear nature of the writing process, writing with sub-band gap light allows the direct patterning of 3-dimensional structures (see Fig. 43.6).

Photosensitivity has been demonstrated within all of the standard glass families, and in many other amorphous thin films (see Sect. 43.2). Because of their large photosensitivity, direct patterning of integrated optics structures in chalcogenide glasses is possible using low power light sources [43.55, 60].

43.1.3 Glass as Host Material

For completeness, it should be mentioned that glasses are unique in their ability to incorporate a wide range of dopants, sometimes in very high concentration. This is related to the random network structure of a glass. Foreign species are much more likely to find a suitable bonding site, or simply space to reside, inside a glass versus a crystal. These foreign species can be rare-earth ions, transition metal ions, or semiconductor or metal nanoparticles, for example. As a result, a glass provides significant scope for active functionality. We can transform a passive glass into a laser glass, a nonlinear optical glass, or a magneto-optic glass, for example, by appropriate doping [43.3, 6].

43.2 Glasses for Integrated Optics

In general, thin films can be amorphous, polycrystalline, or crystalline. *Tien* and *Ballman* [43.45] provided an early review of waveguide results achieved for various materials lying within each of these categories. Unless the crystal grain size is sufficiently small relative to the wavelength of interest [43.47], polycrystalline films are too lossy for integrated optics. It should be noted that high attenuation might be tolerable if circuit length is sufficiently short. The present discussion is concerned with amorphous films, which Tien further subcategorized as low index ($n < 1.7$), medium index ($n < 2$), and high index ($n > 2$). For convenience, we will follow a similar approach in the following sections. This categorization is somewhat arbitrary, especially when considering material systems (such as the silicon oxynitride system) that enable a range of refractive index. It is interesting to note that 1.7 is the approximate upper limit for the refractive index of organic glasses [43.49]

As noted in Sect. 43.1, increased circuit density is one of the primary goals of integrated optics research [43.9]. Whether employing traditional total internal reflection effects or photonic band gap materials, increased density relies on high index contrast between at least two compatible materials. Note that the terminology 'high index' and 'high index contrast' are rather imprecise. For example, in silica PLC technologies core-cladding index differences of $\Delta n \approx 0.02$ have been labeled as 'superhigh' index contrast [43.10]. This is a very small value, however, relative to the index contrasts that characterize SOI photonic wire waveguides [43.30].

43.2.1 Low Index Glassy Films

SiO_2-Based Glasses

As mentioned in the introduction, the SiO_2 on silicon PLC system is the most widely used and developed glass-based integrated optics platform. PLC development (mainly in the 1990s) was driven by fiber optic long haul communication systems, especially the emergence of wavelength division multiplexing (WDM). Various devices, but especially arrayed waveguide grating (AWG) wavelength demultiplexers, were developed to a very high degree of sophistication by the telecommunications industry. Good early [43.18] and recent [43.9,10] reviews are available in the literature. A brief overview of the technology is given below, as it illustrates some of the advantages and challenges associated with glass-based photonic integration.

As mentioned in Sect. 43.1.1, commercial PLC waveguides are fabricated primarily by FHD [43.10] or by CVD [43.9]. In addition, considerable research has been conducted on sol-gel synthesis [43.61], with the aim of reducing fabrication costs and providing greater flexibility over the choice of glass compositions. Typically, the undercladding is pure silica glass. To raise its refractive index, the core layer is doped with Ge or P. Ge-doped SiO_2 is known for its photosensitivity, as discussed in Sect. 43.1.2. Addition of P lowers the viscosity and characteristic reflow temperature, enabling the processing options discussed in Sect. 43.1.1. Typical relative index offset Δ between the core and cladding is in the 0.3 to 2% range, corresponding to minimum waveguide bend radius R in the 2 to 25 mm range [43.10]. After RIE to form an approximately square waveguide core, an upper cladding is deposited and subjected to heat treatment. The upper cladding is often a boro-phosphosilicate glass (BPSG), partly to enable reflow. Further, the B and P dopants have opposite effects on refractive index allowing a nearly symmetric waveguide structure to be obtained.

Given the target applications, it is not surprising that PLC technology placed a great emphasis on efficient coupling between the integrated waveguides and external fiber waveguides. Thus, waveguide cross-sectional dimensions and refractive index contrast between core and cladding layers were tailored to provide a good impedance match (low reflection and good modal overlap) to standard fiber. By employing essentially the same glass (doped SiO_2) as that used to construct fiber, it is even possible to achieve intimate reflowed (fusion type) coupling between the integrated and fiber guides [43.18]. The emphasis on impedance matching is due to the great importance of minimizing insertion loss in fiber systems, but presents some practical limitations:

1. The relatively low index contrast ($\approx 10^{-3}$) between core and cladding necessitates thick glass films. For example the undercladding or buffer layer, often a thermally grown SiO_2 layer, must typically exceed 12 μm in order to negate radiation losses into the high index silicon substrate. Further, high temperature anneals (typically 900–1150 °C) are required to drive out hydrogen impurities and to reflow the core and upper cladding layers. The combination of thick films, high temperature anneals, and thermal expansion mismatch can result in wafer bending and damage to the glass films. This is partly alleviated

in practice by depositing identical layers on both sides of the Si wafer [43.9], which adds cost and complexity.
2. Since modal area and minimum bend radius scale inversely with core-cladding index contrast, traditional PLC waveguides do not support high-density optical integration. As mentioned above, index contrasts in the 0.3 to 2% range correspond approximately to bending radii in the 25 to 2 mm range [43.10].

In recent work at Corning [43.62], very low loss (< 0.1 dB/cm) waveguides and ring resonators were realized in PECVD grown silica-germania waveguides having index contrast as high as 4%. Such high index contrasts can accommodate bending radius of less than 1 mm, which is comparable to the range explored recently by IBM researchers using silicon oxynitride materials [43.63].

Amorphous Aluminium Oxide

Sapphire (crystalline Al_2O_3) is amongst the most important solid-state laser hosts. Alumina (polycrystalline or amorphous Al_2O_3) is an important industrial material in its own right, possessing outstanding mechanical and thermal properties [43.15]. Amorphous Al_2O_3 films are of interest for integrated optics for several reasons [43.47]. First, the refractive index is relatively high (although falling within the low index range specified above), typically $n \approx 1.65$. Second, Al_2O_3 is an excellent host for rare earth and transition metal dopants. As discussed in Sect. 43.3, rare earth dopants of interest are typically trivalent, matching the valency of Al ions in Al_2O_3 [43.64]. As a result, rare earth ions can be incorporated easily into the alumina matrix. In short, Al_2O_3 can homogeneously dissolve large concentrations of rare earth ions and is therefore of interest for realization of integrated amplifiers and light sources. Finally, Al_2O_3 films typically have excellent transparency from the UV to mid-IR range.

Fluoride Glasses

Heavy-metal fluoride glasses (typically fluorozirconate glasses) such as ZBLAN have been widely studied since their discovery in 1974 [43.41]. One of their outstanding attributes is a wide transparency range, extending from the UV well into the mid-IR (see Fig. 43.1). They have received considerable attention as fiber optic materials, because theory predicts a minimum absorption well below that of silica glass. Further, rare earth ions exhibit the greatest number of useful radiative transitions when embedded in fluoride glasses [43.65]. This is due to their wide transparency window and low characteristic phonon energies (see Sect. 43.3).

Fluoride glasses typically have refractive indices in the 1.47–1.57 range, which is advantageous in terms of being well matched to silica glasses. Thin film deposition of these complex multicomponent glasses is difficult, and thermal expansion mismatches with standard substrates create further challenges. For these reasons, fluoride glasses have not been widely explored for applications in integrated optics. The so-called PZG fluoride glasses ($PbF_2 - ZnF_2 - GaF_3$) have been successfully deposited using straightforward evaporation techniques, enabling relatively low loss waveguides and erbium-doped amplifiers on a silicon platform [43.66].

43.2.2 Medium Index Glassy Films

Silicon Oxynitride

Silicon oxynitride (SiON) films are generally deposited by a CVD technique. The promise of this material system for integrated optics was identified in early work [43.45]. One of the main attributes of SiON is that it is a standard material system employed in silicon microelectronics, and the thin film technology has been developed accordingly [43.47, 63]. Because of this, SiON is currently being studied as potential material for on-chip interconnects [43.50]. Further, the system enables a continuous range of refractive index from approximately 1.45 (SiO_2) to 2 (Si_3N_4) at 1550 nm wavelength. This index range has been extended to approximately 2.2 by deposition of non-stoichiometric, silicon-rich nitride films [43.67]. SiON and SiN have been amongst the most explored materials for realization of microring resonator structures [43.53, 67].

As an optical material, SiON has some drawbacks. The main one is the presence of hydrogen impurities in films deposited by traditional techniques. Overtones due to hydrogen bonds (mainly N–H and O–H) can produce impractically large values of loss in the 1300 nm and 1550 nm telecommunications bands [43.62]. Long term, high temperature annealing (typically at $>1000\,^{\circ}C$) is required to reduce this loss. Interestingly, structural relaxation on the time scale of hours and days has been observed in such annealed films [43.47]. Perhaps related to this metastability, UV light has been used as a means to trim the refractive index of SiN-based microring resonators [43.53]. Modified deposition processes that can produce SiON films having low stress and low hydrogen content (without requiring a high temperature annealing step) have been reported recently [43.63, 67]. However,

inherent film stress can limit the maximum thickness to a few hundred nanometers in some cases [43.50].

43.2.3 High Index Glassy Films

Amorphous Metaloxides

Many amorphous metaloxides (Y_2O_3, Nb_2O_5, Ta_2O_5, etc.) have traditionally been used as high index layers in optical thin film stacks [43.49]. It is logical to look at these materials in the hunt for high index thin films for integrated optics. Often these oxides are miscible with SiO_2, making it possible to tune the refractive index and other material properties over a range of values (as in the case of silicon oxynitride) [43.69].

TiO_2 films are used as dielectric layers, optical coatings, and to protect underlying materials from mechanical damage or corrosion [43.47]. The high dielectric constant of TiO_2 is widely exploited in microelectronics applications. It also has useful optical properties, including a refractive index as high as 2.6 (depending on film deposition details) and good transparency from the UV to mid-IR. The TiO_2–SiO_2 material system has good properties for sol-gel synthesis of thin films [43.61]. Integrated waveguides based on TiO_2 have been studied [43.47, 69], and AWG devices in TiO_2-rich oxide glass with $n \approx 1.9$ were recently reported [43.70].

Ta_2O_5 (With $n \approx 2.1$) is another well-studied material, used for example as a high dielectric constant material in microelectronics. It has low absorption in the visible to near infrared wavelength range, and has been recently studied as a material for active integrated optics [43.71,72]. Further, Ta_2O_5/SiO_2 has been applied to the study of compact microring resonators [43.73].

TiO_2 and Ta_2O_5 have been used in the fabrication of three-dimensional photonic crystals with fundamental bandgaps in the visible and near infrared [43.68,74]. An example is shown in Fig. 43.7.

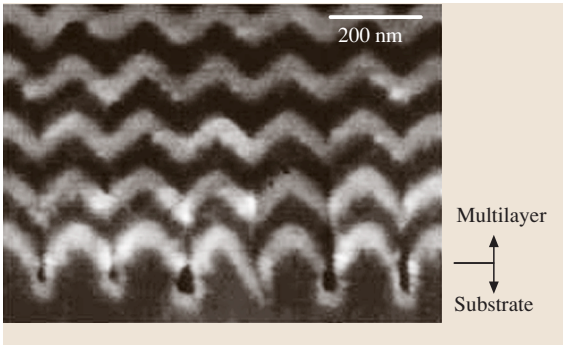

Fig. 43.7 A three-dimensional photonic crystal fabricated using the autocloning growth technique is shown. The *bright* and *dark* layers are TiO_2 and SiO_2 glass, respectively [43.68]

Heavy Metal Oxide Glasses

These glasses are based primarily on the oxides of bismuth (Bi_2O_3) and lead (PbO). They have relatively low phonon energies and transmit further into the infrared than most oxide glasses [43.75]. They also have interesting magneto-optic [43.6] and nonlinear optical [43.3] properties.

Chalcogenide Glasses

Many chalcogenide alloys, based on S, Se, or Te, are excellent glass formers. In fact, Se is the only element able to easily form a glass on its own [43.14]. These glasses are characterized by very low phonon energies, good transparency in the mid-infrared, and a wide array of beam-induced structural changes [43.51]. Further, chalcogenide glasses are essentially amorphous semiconductors, with electronic absorption edge typically in the visible to near infrared. Related to this, they have very high refractive indices, ranging from 2.2 for sulfide glasses to greater than 3 for some telluride glasses. They are currently of industrial interest for night-vision optics [43.38], fibers for infrared transmission [43.41], and optical and electronic memory elements [43.51].

Chalcogenide glasses have many appealing features for integrated optics. High quality thin films can often be deposited by straightforward techniques such as evaporation or sputtering. Their high indices make them suitable for realization of compact waveguides [43.55] and photonic crystals [43.76]. Their beam-induced properties enable many unique processing options. Some chalcogenide alloys have good potential as laser glasses [43.41], with the ability to uniformly dissolve large concentrations of rare-earth ions. Perhaps of greatest interest, the chalcogenide glasses are amongst the most promising materials for nonlinear integrated optics [43.77, 78]. On this last point, several chalcogenide glasses have ultrafast optical Kerr response 2 to 3 orders of magnitude higher than that of SiO_2, while satisfying basic figure of merit criteria for all-optical switching. Results for metal-doped chalcogenide glasses [43.78] suggest even higher nonlinearities might be attainable. Combined with the possibility of realizing highly confining waveguides, this makes chalcogenide glasses one of few material systems that can realistically satisfy long-standing goals for nonlinear processing in integrated optical circuits. For example, it has been estimated [43.77]

that 1 pJ pulses of 1 ps duration ($\approx$ 1 W peak power) could induce phase shifts (due to self phase modulation) greater than π in feasible chalcogenide glass waveguides with length on the order of a few centimeters. This is predicated on realization of low loss waveguides with modal area of $\approx 1\,\mu m^2$. Recent experimental results suggest that this goal is within reach [43.55].

Tellurite Glasses

While TeO_2 is a conditional glass former, the addition of other oxides can result in stable glasses with many interesting properties [43.75]. They typically have refractive index greater than 2, low phonon energy, large optical nonlinearities, and a high acousto-optic figure of merit. Further, they have been widely studied as hosts for rare-earth ions. Of particular interest has been the wide bandwidth of the 1550 nm emission exhibited by erbium in tellurite glass [43.79]. Because of these numerous attractive properties, tellurite glasses and amorphous TeO_2 films ($n \approx 2.2$) have received some attention for applications in integrated optics [43.80].

43.3 Laser Glasses for Integrated Light Sources

Active functionality includes means to generate and detect light (especially stimulated emission and absorption) and means to control (switch, modulate, etc.) light signals. Numerous material properties are employed in active photonics, including thermo-optic, acousto-optic, magneto-optic, electro-optic, and nonlinear Kerr effects. Many glasses have attractive thermo-optic or acousto-optic properties, and a few examples were cited in Sect. 43.2. Also in Sect. 43.2, some glasses with promising nonlinear optical properties were discussed. Elsewhere in this volume, K. Tanaka has provided an excellent review of nonlinearities in photonic glasses. A recent, thorough review of magneto-optic glasses is also available [43.6].

Arguably, the most critical element for photonic integration is an integrated light source. Rare-earth doped glasses are well-established laser media, used especially for the realization of bulk and fiber lasers. Considerable effort has been directed towards development of integrated amplifiers and lasers based on such glasses. In the following, we attempt to highlight some ways in which light sources based on glasses are uniquely enabling, relative to those based on crystalline materials. The performance advantages discussed below combined with the properties discussed in earlier sections (fabrication options) make glasses particularly attractive.

43.3.1 Advantages of Glass-based Light Sources

Stimulated emission devices in glass are almost always based on trivalent rare-earth dopants [43.6]. Thus, the term laser glass can usually be equated with the term rare-earth doped glass. Rare-earth doped laser glasses have been widely studied and reviewed [43.64, 65]. Further, recent and comprehensive reviews on Nd- and Er-doped integrated glass amplifiers and lasers are available [43.6, 81]. Relative to single crystal hosts, glass hosts result in rare-earth ions exhibiting broadened luminescence lines and lower peak stimulated emission cross-sections [43.65]. This property is a result of the random network structure of glasses; embedded rare earth ions exist in a range of local environments. The broadened, weaker emission is of great importance for the realization of broadband, low noise fiber amplifiers.

It should be noted that the semiconductor injection laser is an extremely advanced technology, and is the dominant type of integrated light source at present and for the foreseeable future. Semiconductor lasers have important advantages over any glass-based device demonstrated to date. First, semiconductor gain media typically have gain coefficients of the order $\approx 100\,cm^{-1}$ [43.17]. By comparison, glasses require high rare-earth dopant concentration to achieve gain coefficients exceeding $1\,cm^{-1}$. Thus, semiconductor optical amplifiers (SOAs) and lasers have cavity lengths measured in tens to hundreds of μm while it is typical for glass waveguide amplifiers and lasers to be measured in cm. Second, semiconductor light sources are pumped electrically while glass devices are typically pumped optically. Electrical pumping is highly desirable for optoelectronic integration of photonic devices on electronic chips. However, as discussed below, integrated glass waveguide lasers have important advantages of their own [43.82].

The lifetime of the metastable lasing level in rare-earth doped glasses is usually on the order of ms, much longer than the ns lifetimes typical of semiconductor gain media. This long lifetime implies that the gain does not change rapidly with variations in input power (pump

or signal). This is an essential feature of the commercially important erbium-doped fiber amplifier (EDFA); the long lifetime (≈ 10 ms) of the $^4I_{13/2}$ level of erbium in silicate glass contributes to low noise operation, high pump efficiency, and low crosstalk between wavelength channels in a WDM system [43.83]. Further, since the relaxation oscillations in glass waveguide lasers occur at relatively low frequency, glass lasers can be modelocked at correspondingly much lower repetition rates compared to semiconductor lasers [43.82]. This can enable much higher peak intensities from the glass laser.

Related to the discussion in Sect. 43.1, lower cavity loss (higher cavity Q) is generally possible for glass devices. Further, the long metastable lifetime of the rare-earth transition allows glass lasers to have linewidths approaching the Schawlow–Townes limit [43.84]:

$$\Delta\nu = \frac{2\pi h\nu_0\,(\Delta\nu_c)^2}{P}\left(\frac{N_2}{N_2 - N_1}\right) \qquad (43.8)$$

where ν_0 is the laser center frequency, P is the laser output power, N_2 and N_1 are the population densities of the upper and lower lasing levels, and $\Delta\nu_c = (1/2\pi t_c)$ with t_c the photon lifetime in the cavity. The high Q of glass laser cavities coupled with relatively high output powers enables linewidths less than 10 kHz, orders of magnitude below that of semiconductor DFB lasers [43.82]. The high cavity Q and long metastable lifetime is also advantageous for achieving ultrastable passive mode locking, with low timing jitter and pulse-to-pulse power variation.

Finally, glasses offer the possibility of integration on various substrates. While semiconductor lasers are inherently integrated structures, they are not easily transportable between platforms. For example, III-V semiconductor lasers have not shown great promise (in spite of heroic efforts in some cases) to satisfy the desire for a compact, truly integrated light source on the silicon electronics platform. Glasses (perhaps doped with semiconductor nanocrystals) are increasingly viewed as the more promising route to achieving such a goal [43.64].

43.3.2 Alternative Glass Hosts

The theoretical maximum gain (cm^{-1}) of a rare-earth doped glass waveguide amplifier can be expressed [43.81] as $\gamma_p = \Gamma\sigma_p N_{RE}$, where σ_p is the peak (versus wavelength) stimulated emission cross-section (cm^2) for the transition of interest and N_{RE} is the volume density (cm^{-3}) of the rare-earth ions. Γ is a dimensionless factor (lying between 0 and 1) that accounts for the spatial overlap of the waveguide mode (at the wavelength to be amplified) and the active ions producing the gain. It can be optimized through waveguide design, irrespective of the glass host, and will not be considered further here. The expression for γ_p neglects all waveguide losses (due to scattering, etc.) and assumes that all of the rare-earth ions have been promoted to the desired lasing level; i. e. a complete population inversion. It is therefore an ideal and unattainable limit, but is useful for framing the following discussion.

Since compactness is a central goal of integrated waveguide lasers, alternative glass hosts can be compared on the basis of the maximum gain (γ_{max}) that they enable in practice (for a given transition of a given rare-earth ion). Further, since low noise operation relies on a near complete population inversion [43.81], it is desirable that $\gamma_{max} \approx \gamma_p$. In simple terms, the glass should dissolve a large concentration of the rare earth ion (high N_{RE}), should result in a large stimulated emission cross-section for the desired transition, and should enable the realization of a nearly complete population inversion. The importance of other practical considerations, such as stability, processing options, and physical properties of the glass, will depend on the intended application. Some hosts provide unique advantages, such as flexible pumping options, as discussed in Sect. 43.3.3.

As mentioned, laser transitions in glasses are generally provided by radiative decay between two energy levels of a trivalent rare-earth ion. Perhaps the most important example is the $^4I_{13/2}$ to $^4I_{15/2}$ transition of Er^{3+}, which produces luminescence in the 1500–1600 nm wavelength range. Once an ion has been promoted (by pumping) to the upper lasing level, it will eventually transition to another state by interactions with the glass, impurities in the glass, the photon fields (at the signal or pump wavelength), or with other rare-earth ions in its vicinity [43.65]. The metastable lifetime of the upper lasing level can be expressed [43.81]

$$\frac{1}{\tau} = A + W_{MP} + W_{ET} + W_{IMP} \qquad (43.9)$$

where A is the effective rate of spontaneous radiative decay to all lower lying levels, W_{MP} is the rate of non-radiative decay due to multi-phonon energy exchanges with the glass, W_{ET} is the rate of non-radiative energy transfer due to interactions between closely spaced rare-earth ions, and W_{IMP} is the rate of energy transfer to quenching impurity centers in the glass. The first three terms on the right will be discussed below. For the last term, a classic example is the quenching of the 1550 nm luminescence band of erbium due to resonant energy transfer to OH^- impurities in silica glass [43.65].

The choice of a particular glass host will impact several important properties of a given transition: pumping efficiency, peak gain, linewidth, metastable lifetime, etc. Alternative glasses can be compared on the basis of a few key parameters, as discussed in the following sub-sections. Representative data for erbium in various glasses is given in Table 43.1.

Stimulated Emission Cross-Section

Stimulated transitions of rare-earth ions in glass tend to be predominately driven by electric dipole interactions [43.65]. For a given transition of interest, the spontaneous emission probability can be expressed in cgs units as [43.6, 85]:

$$A = \frac{64\pi^4 e^2 \chi}{3h\,(2J+1)\,\lambda_p^3} S \qquad (43.10)$$

where J is the total angular momentum of the upper lasing level, λ_p is the peak emission wavelength, and χ is the local field correction factor. For electric-dipole interactions of an ion in a dielectric medium, $\chi \approx n(n^2+2)^2/9$, with n the refractive index of the host glass. S is the quantum-mechanical line strength for the transition. Further, the peak stimulated emission cross-section can be expressed in terms of the spontaneous emission probability:

$$\sigma_p = \left(\frac{\lambda_p^4}{8\pi c n^2 \Delta\lambda_{eff}}\right) A \qquad (43.11)$$

where $\Delta\lambda_{eff}$ is the effective linewidth of the transition. From (43.10) and (43.11), the host-dependent factors that influence σ_p are the refractive index, the line strength, the effective linewidth, and to a lesser extent the peak emission wavelength (which typically varies only slightly between different hosts). The local field correction factor is significant in hosts with large refractive index, and can result in an enhancement of the stimulated emission cross-section and a reduction of the radiative lifetime. This is especially true for chalcogenide glass hosts, which typically have refractive index in the 2 to 3 range.

Metastable Lifetime

In the limit of low rare-earth dopant concentration, W_{ET} in (43.9) is zero because the ions are sufficiently well separated to negate their interaction. If the difference in energy between the upper lasing level and the adjacent state is several times the effective phonon energy, then W_{MP} can be neglected to first order. Further neglecting impurity quenching, we can then assert that $\tau_0 \approx 1/A$, where τ_0 is the metastable lifetime in the limit of low rare-earth concentration. From Einstein's relations, $A \approx \sigma_p$, so it follows that $\tau_0 \approx 1/\sigma_p$. In short, hosts that result in an enhancement of the peak stimulated emission cross-section (due to an enhancement of the electric-dipole interaction or because of a high local field correction factor) will also result in a reduction in metastable lifetime. In other words, both stimulated and spontaneous emission rates are enhanced.

The inverse scaling of stimulated emission cross-section and metastable lifetime represents a tradeoff, as it is generally desirable for the lifetime to be as large as possible. Some of the advantages of long lifetime were discussed in Sect. 43.3.1. In addition, the pumping efficiency (gain per applied pump power) of a waveguide amplifier scales directly with τ [43.6, 81] and, therefore, the threshold for CW lasing scales inversely with τ [43.86].

Concentration Quenching

Glasses differ greatly in the amount of a given rare-earth dopant that they are able to dissolve. To avoid problematic ion–ion interactions, the rare-earth ions should be

Table 43.1 Representative parameters for erbium ions embedded in various types of glass (after [43.61, 64, 65])

Glass host	Refractive index n	Peak stimulated emission cross-section σ_p (10^{-21} cm^2)	Metastable lifetime τ (ms)	Quenching concentration ρ_q (10^{20} cm^{-3})	Effective luminescence bandwidth (nm)
Silica	1.46	7	12	–	11
Amorphous Al_2O_3	1.64	6	7.8	–	55
Aluminosilicate	1.5	5.7	10	3.9–6.0	43
Phosphate	1.56	8	10	3.9–8.6	27
Fluoride	1.53	5	9	3.8–5.3	63
Tellurite	2.1	13	3.3	–	80
Sulfide	2.4	20	2.5	3.2	–

incorporated homogeneously into the glass structure. In the extreme case of high concentration, the rare-earth ions will form microscopic clusters (phase separation). Such clustering is highly detrimental, as typically all of the ions within a cluster are effectively removed from the desired stimulated emission process [43.81]. As is well known [43.64, 65], the onset of clustering occurs at quite small values (≈ 0.1 at %) in pure silica glass. The addition of Al_2O_3 to SiO_2 allows silica-based fibers to dissolve a significantly higher concentration. For example, a value of 10–20 for the Al ion to Er ion concentration ratio has been shown to greatly reduce clustering of Er ions in silica glass [43.86]. Interestingly, the addition of Ga (with similar ratio) to chalcogenide glasses has been shown to provide a similar reduction in rare-earth ion clustering [43.41]. These additives essentially modify the glass network, and create sites for isolated rare-earth ions to be incorporated. For similar reasons, multicomponent alumino-silicate and phospho-silicate glasses have been favored in the development of integrated waveguide amplifiers, where the rare-earth concentration must be orders of magnitude higher than in fibers [43.81].

Even in the absence of significant clustering, ion–ion interactions can occur at high concentrations. This is simply due to the reduction in inter-ion spacing, and is exacerbated by any non-uniform (non-homogeneous) distribution of the rare-earth ions in the glass host. These interactions are manifested by a reduction in the metastable lifetime, often well described by the semi-empirical expression [43.61, 65]:

$$\tau(\rho) = \frac{\tau_0}{1 + (\rho/\rho_Q)^p} \qquad (43.12)$$

where ρ is the rare-earth ion concentration, ρ_Q is the so-called quenching concentration, and p is a fitting parameter ($p \approx 2$ for interactions between pairs of ions). The parameter ρ_Q is useful for comparing glasses in terms of their ability to uniformly dissolve a given ion.

Phonon Energies

The characteristic phonon energies of a glass depend on the weights of its constituent atoms and the strength and nature (ionic or covalent) of its bonds. Typical values are shown in Table 43.2. The rate of multi-phonon decay (WMP) between two energy levels depends exponentially on the number of phonons required to bridge the energy gap. Thus, the phonon energy has a great impact on the ultimate efficiency of a desired radiative transition. Low phonon energy can be a good or bad thing, depending on the transition of interest and the particular pumping scheme.

Mid- to far-infrared transitions of rare-earth ions can exhibit reasonably high quantum efficiency in low phonon energy hosts, such as fluoride, tellurite, and especially chalcogenide glasses. If the same ions are embedded in silicate or phosphate glasses, these transitions are completely quenched by non-radiative processes at room temperature. For this reason, rare-earth doped chalcogenide glasses are of interest for realization of long wavelength amplifiers and lasers [43.41, 64]. Also unique to low phonon energy hosts is the possibility of efficient upconversion lasers [43.87]. In simple terms, the long lifetimes of numerous energy levels allows processes such as ion–ion interactions and excited state absorption (ESA) to efficiently populate the higher energy levels. By contrast, these levels are rapidly depopulated by phonons in oxide glasses. On the other hand, population of the higher levels is highly detrimental if the desired transition is between two lower levels. For example, the efficient pumping of EDFAs using 980 nm wavelength sources relies on the rapid decay (via multiphonon processes) of ions from the $^4I_{11/2}$ pumping level to the $^4I_{13/2}$ lasing level. In fluoride and chalcogenide glass hosts, ions raised above the $^4I_{11/2}$ level tend to become trapped in higher levels (so-called 'population bottlenecking' [43.65]). Cerium co-doping has been shown to alleviate this problem [43.66]. Another approach is addition of light elements to the glass network, to increase the phonon energy [43.79].

43.3.3 Progress Towards Integrated Light Sources in Glass

Per the preceding discussion, important goals for glass-based lasers include size reduction and the need for simplified optical or (ideally) electrical pumping

Table 43.2 Characteristic maximum phonon energies for a variety of glass hosts (after [43.6, 65])

Glass host	Phonon energy (cm^{-1})
Borate	1400
Phosphate	1200
Silicate	1100
Germanate	900
Tellurite	700
Heavy-metal fluoride	500
Chalcogenide (sulfide)	450
Chalcogenide (selenide)	350

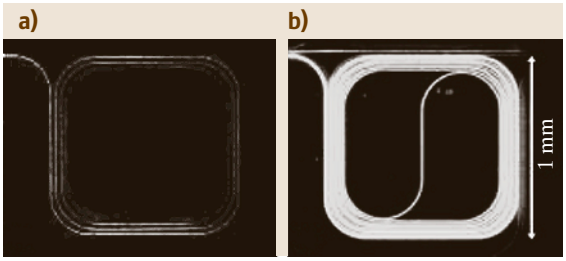

Fig. 43.8 Spiral geometry demonstrated for Al_2O_3-based waveguide amplifiers, where erbium was introduced by ion implantation (*left*) and co-sputtering (*right*). The bright green emission is a result of ion–ion interactions causing up-conversion for the co-sputtered sample [43.89]

schemes. It should be noted that integration brings its own advantages. As is well known, waveguide lasers have greatly enhanced pump efficiency (gain per applied pump power) relative to their bulk solid-state counterparts. This is due to the confinement of the pump beam and the stimulated emission beam within a small volume. As explored recently in [43.88], this benefit scales with confinement. Amplifiers based on very high index contrast waveguides can have extremely high pump efficiency, as well as requiring only a small amount of wafer real estate. Thus, while the gain per unit length is limited by concentration quenching in rare-earth doped glasses, devices can still be very compact through the use of folded spiral waveguide layouts as illustrated in Fig. 43.8 [43.89].

In terms of maximizing gain per unit length, phosphate glasses have produced the best results to date. This is due to their ability to uniformly dissolve large concentrations of rare-earth ions, and the high cross-sections exhibited by those ions. The high phonon energy can also be an advantage as discussed above. Phosphate glass disks (typically ≈ 1 mm thick) have been widely used for realization of compact microlasers [43.90] and ultrafast modelocked lasers with pulse length as short as 220 fs [43.91] and repetition rate exceeding 40 GHz [43.92]. Phosphate glass fiber lasers with a length of only 7 cm have recently generated 9.3 W of output power [43.93]. Sputtered phosphate glass waveguides have produced gains exceeding 4 dB/cm [43.94]. More recently, a phosphate glass co-doped with 8 at % erbium and 12 at % ytterbium was used to realize ion-exchange waveguides exhibiting 4.1 dB gain in only 3 mm length [43.95]. At such high concentrations, the rare-earth constituents can hardly be called dopants as they exceed the concentration of some of the host glass constituents.

On the theme of simplified pumping options, so-called broadband sensitizers [43.96] are of great interest. A broadband sensitizer is essentially a co-dopant that is able to efficiently absorb pump energy over a wide wavelength range and subsequently excite nearby rare-earth ions to the desired lasing level. This might enable planar waveguide amplifiers that are pumped transversely using low cost broadband light sources [43.64]. Silicon nanoclusters (embedded in oxide glass) are receiving the most attention at present. In addition to acting as a broadband sensitizer, there is evidence that these nanoclusters can enhance the stimulated emission cross-section of co-doped rare-earth ions by 1–2 orders of magnitude. *Han* et al. [43.97] have reported a waveguide amplifier (on a silicon platform) exhibiting signal enhancement of 7 dB/cm, in spite of a very low erbium concentration. The same group has also reported gain using transverse pumping by LED arrays [43.98]. Finally, the presence of a large concentration of silicon clusters makes electrical pumping a realistic possibility for some silicon-rich oxide glasses [43.64].

It seems very likely that chip-scale glass-based lasers are on the verge of playing a central role in photonics. These lasers will deliver moderate power in a very small package, and will offer extreme spectral purity or stable, high-repetion rate pulses. They might even satisfy the long-standing desire for a silicon-based laser [43.64, 91], facilitating the convergence of photonics and electronics.

43.4 Summary

Glasses have numerous advantages (ease of component fabrication, low scattering loss, flexible atomic structure) that have made them the workhorse material for traditional bulk optics applications. These properties can provide equal or greater advantage in the realization of microphotonic devices and circuits. The glass transition can enable manufacturing techniques unavailable to other materials, and realization of devices having surface roughness approaching fundamental limits. Owing to this, glasses underlie the highest Q microcavities and some of the lowest loss photonic crystal and microphotonic waveguides reported to date. The metastability

of glass enables a rich array of processing and post-processing options. Direct patterning of waveguides, gratings, and other microphotonic elements by energetic beams is widely studied. These methods of material modification are also promising for post-fabrication trimming of devices. On the other hand, metastability has implications for processing and aging of glass devices.

Rare-earth doped glasses offer numerous advantages relative to other solid-state laser media, especially for realization of ultra-low noise single frequency and ultrafast lasers. Recent advances have greatly increased the maximum gain per unit length, and point to the potential for compact, on-chip glass-based light sources. Progress with respect to 2nd and 3rd order nonlinear effects in glasses is ongoing. It is expected that cm-scale switching or pulse shaping devices based on glasses will become feasible, at least for niche applications.

Overall, it is clear that glasses can contribute greatly to the development of compact, low-loss, multifunction optics integrated with electronics.

Defining Terms

Amorphous Metaloxides are glassy alloys of a transition metal with oxygen, typical examples being TiO_2, Ta_2O_5, Nb_2O_5, and Y_2O_3. In bulk form, these materials are typically polycrystalline or crystalline ceramics. However, amorphous thin films can be deposited with relative ease, and they have been widely used as high index layers in optical filter design and as dielectric layers in the microelectronics industry.

Broadband Sensitizer is typically some species co-doped along with rare-earth ions into a glass host, in order to increase the pumping efficiency or radiative efficiency of the rare-earth ions. Various sensitizers have been demonstrated, including silicon nanoclusters, silver ions, and other rare earth ions (such as in the sensitization of erbium by ytterbium).

Chalcogenide Glasses are amorphous alloys containing S, Se, and/or Te. Typical examples include Se, GeS_2, $GeSe_2$, As_2S_3, As_2Se_3, and As_2Te_3. By intermixing these and other binary chalcogenide glasses, a wide variety of multicomponent glasses can be formed. Further, a wide range of non-stoichiometric compositions is possible. Several compositions have become standard industrial materials, including $Ge_{33}As_{12}Se_{55}$ and $Ge_{28}Sb_{12}Se_{60}$. The chalcogenide glasses are characterized by narrow bandgaps and good transparency in the mid to far infrared wavelength range.

Concentration Quenching refers to the reduction in luminescence efficiency and luminescence lifetime of a laser glass when the rare-earth dopant concentration is high. Quenching is due to interactions between closely spaced rare-earth ions at high concentrations. These interactions create new pathways, other than the desired radiative decay, for the ions to relax to the ground state after they have been raised to a desired lasing level by pump energy.

Devitrification refers to the transition of a glassy material to its lower energy crystalline state. This process is usually driven by thermal energy, such as if the material is held at some characteristic temperature above its glass transition temperature. The difference between the crystallization temperature and the glass transition temperature for a particular glass is one measure of its stability.

Fluoride Glasses are multicomponent glasses, typically based on fluorides of zirconium, barium, lead, gallium, lanthanum, aluminium, and sodium. They have a wide transparency range, from ultraviolet to mid-infrared wavelengths. They also have low characteristic phonon energies and can dissolve large concentrations of rare-earth ions. For these reason, they are extremely popular as hosts for rare-earth doped amplifiers and lasers operating in the UV-vis and mid-infrared regions.

Glass Transition Temperature is the approximate temperature at which a material changes from a supercooled liquid to an amorphous solid, or vice versa. The transition is marked by an abrupt but continuous change in slope of the specific volume and enthalpy versus temperature curves. Viscosity varies rapidly near the glass transition temperature, which is also sometimes called the softening temperature.

High Index Contrast refers to waveguides or devices fabricated using two or more materials that have very different refractive index. High index contrast is the basis for the confinement of light to very small cross-sectional area waveguides or very small volume optical cavities, either using total internal reflection or photonic bandgap effects. High index contrast thus is the basis for increased density of optical integrated circuits.

Integrated Optics/Photonics refers to the manufacture of photonic elements and circuits on a planar substrate, typically using thin film deposition, lithography, and etching steps. Typically, the substrate is a glass or semi-

conductor wafer and the photonic elements are guided wave devices.

Metastability is a term that refers to the non-equilibrium nature of glasses or amorphous solids. Amorphous solids have excess internal energy relative to the corresponding crystalline state or states of the same material. The method of manufacture, such as melt quenching, inhibits a transition to the lowest energy crystalline state.

Microphotonics refers to the chip-scale manufacture of optical and photonic waveguide circuitry, using processing techniques borrowed from the microelectronics industry. Related to this is the need for high-density integrated optics, as facilitated by high index contrast waveguides and photonic crystals. By usual definition, microphotonics refers specifically to the monolithic manufacture of optical and photonic elements on silicon (CMOS) chips.

Photoinduced Effects are changes in the properties of a glass induced by light, involving transitions between metastable states of the glass or changes in defect sites within the glass. Typically, a laser beam is used to locally modify the refractive index, density, absorption coefficient, etc. of the glass. These processes are widely used to pattern photonic structures such as Bragg gratings, waveguides, and refractive lenses into glasses.

Planar Lightwave Circuit or PLC refers to the industrially established processes for manufacturing integrated optics devices in silica-based glasses deposited on silicon wafers. Typically, the glass layers are deposited by chemical vapor deposition or flame hydrolysis. These technologies were developed mainly for applications in fiber optics, and are widely used to manufacture wavelength multiplexers.

Reflow is the process of heating a glass above its glass transition temperature, to the point that its viscosity is sufficiently reduced to enable the material to flow. In combination with surface tension effects or other external forces, reflow is often exploited in the reshaping of optical devices.

Supercooling Temperature is the difference between the glass transition temperature and the in-use temperature for a glass-based device. For a large (small) supercooling temperature, the structural relaxation rate is low (high).

Structural Relaxation is essentially an aging effect associated with glasses. Because glasses are metastable materials with random network structures, they are inherently subject to short or long term changes in material properties. Often, structural relaxation is manifested by a change in specific volume (densification) at fixed temperature versus time. The rate of such changes is extremely sensitive to the difference between the glass transition temperature and the observation temperature. Structural relaxation can be induced rapidly by an annealing step, in which the glass is heated near its glass transition temperature for some period of time.

References

43.1 H. Rawson: Glass and its History of Service, Part A, IEE Proceedings **135**(6), 325–345 (1988)

43.2 W. J. Tropf, M. E. Thomas, T. J. Harris: *OSA Handbook of Optics, Vol. II*, 2nd edn. (McGraw-Hill, New York 1995)

43.3 K. Hirao, T. Mitsuyu, J. Si, J. Qiu: *Active Glass for Photonic Devices, Photoinduced Structures and Their Application* (Springer, Berlin, Heidelberg 2001)

43.4 Z. Yin, Y. Jaluria: Neck-down and thermally induced defects in high-speed optical fiber drawing, J. Heat Transfer **122**(2), 351–362 (2000)

43.5 W. A. Gambling: IEEE J. Sel. Top. Quant. Elec. **6**, 1084 (2000)

43.6 M. Yamane, Y. Asahara: *Glasses for Photonics* (Cambridge Univ. Press, Cambridge 2000)

43.7 J. Lucas: Curr. Op. Sol. St. Mat. Sci. **4**, 181 (1999)

43.8 H. Ma, A. K.-Y. Jen, L. R. Dalton: Adv. Mat. **14**, 1339 (2002)

43.9 M. R. Poulsen, P. I. Borel, J. Fage-Pederson, J. Hubner, M. Kristensen, J. H. Povlsen, K. Rottwitt, M. Svalgaard, W. Svendsen: Opt. Eng. **42**, 2821 (2003)

43.10 K. Okamoto: *Integrated Optical Circuits and Components, Design and Applications* (Dekker, New York 1999), Chapt. 4

43.11 S. Torquato: Nature **405**, 521 (2000)

43.12 P. G. Debenedetti, F. H. Stillinger: Nature **410**, 259 (2001)

43.13 C. A. Angell, K. L. Ngai, G. B. McKenna, P. F. McMillan, S. W. Martin: J. Appl. Phys. **88**, 3113 (2000)

43.14 J. M. Saiter, M. Arnoult, J. Grenet: Phys. B: Cond. Matt. **355**, 370 (2005)

43.15 J. C. Anderson, K. D. Leaver, R. D. Rawlings, J. M. Alexander: *Materials Science*, 4th edn. (Chapman Hall, London 1990)

43.16 B. Hendriks, S. Kuiper: IEEE Spectrum **41**, 32 (2004)

43.17 G. P. Agrawal: *Fiber-Optic Communication Systems*, 2nd edn. (Wiley, New York 1997)
43.18 Y. P. Li, C. H. Henry: IEE Proc.-Optoelectron **143**, 263 (1996)
43.19 R. R. A. Syms, W. Huang, V. M. Schneider: Elec. Lett. **32**, 1233 (1996)
43.20 R. R. A. Syms, A. S. Holmes: IEEE Phot. Tech. Lett. **5**, 1077 (1993)
43.21 T. J. Kippenberg, S. M. Spillane, B. Min, K. J. Vahala: IEEE J. Sel. Top. Quant. Elec. **10**, 1219 (2004)
43.22 D. W. Vernooy, V. S. Ilchenko, H. Mabuchi, E. W. Streed, H. J. Kimble: Opt. Lett. **23**, 247 (1998)
43.23 M. L. Gorodetsky, A. A. Savchenkov, V. S. Ilchenko: Opt. Lett. **21**, 453 (1996)
43.24 L. Tong, R. R. Gattass, J. B. Ashcom, S. He, J. Lou, M. Shen, I. Maxwell, E. Mazur: Nature **426**, 816 (2003)
43.25 P. J. Roberts, F. Couny, H. Sabert, B. J. Mangan, D. P. Williams, L. Farr, M. W. Mason, A. Tomlinson, T. A. Birks, J. C. Knight, P. St. J. Russell: Opt. Express **13**, 236 (2005)
43.26 C.-T. Pan, C.-H. Chien, C.-C. Hsieh: Appl. Opt. **43**, 5939 (2004)
43.27 M. He, X.-C. Yuan, N. Q. Ngo, J. Bu, V. Kudryashov: Opt. Lett. **28**, 731 (2003)
43.28 M. He, X.-C. Yuan, J. Bu: Opt. Lett. **29**, 2004 (2004)
43.29 Y. A. Vlasov, S. J. McNab: Opt. Express **12**, 1622 (2004)
43.30 F. Grillot, L. Vivien, S. Laval, D. Pascal, E. Cassan: IEEE Phot. Tech. Lett. **16**, 1661 (2004)
43.31 T. Barwicz, H. I. Smith: J. Vac. Sci. Tech. B **21**, 2892 (2003)
43.32 D. K. Armani, T. J. Kippenberg, S. M. Spillane, K. J. Vahala: Nature **421**, 925 (2003)
43.33 V. Van, P. P. Absil, J. V. Hryniewicz, P.-T. Ho: J. Light. Tech. **19**, 1734 (2001)
43.34 K. J. Vahala: Optical Microcavities, Nature **424**, 839–851 (August 2003)
43.35 S. J. McNab, N. Moll, Y. A. Vlasov: Opt. Express **11**, 2927 (2003)
43.36 P. K. Gupta, D. Inniss, C. R. Kurkijian, Q. Zhong: J. Non-Crystalline Sol. **262**, 200 (2000)
43.37 D. P. Bulla, W.-T. Li, C. Charles, R. Boswell, A. Ankiewicz, J. Love: Appl. Opt. **43**, 2978 (2004)
43.38 X. H. Zhang, Y. Guimond, Y. Bellec: J. Non-crystalline Sol. **326&327**, 519 (2003)
43.39 A. K. Mairaj, X. Feng, D. P. Shepherd, D. W. Hewak: Appl. Phys. Lett. **85**, 2727 (2004)
43.40 A. K. Mairaj, R. J. Curry, D. W. Hewak: Appl. Phys. Lett. **86**, 094102 (2005)
43.41 J. S. Sanghera, L. B. Shaw, I. D. Aggarwal: *Rare-Earth-Doped Fiber Lasers and Amplifiers*, 2nd edn. (Dekker, New York 2001), Chapter 9
43.42 Z. Zhang, G. Xiao, C. P. Grover: Appl. Opt. **43**, 2325 (2004)
43.43 P. K. Tien: Appl. Opt. **10**, 2395 (1971)
43.44 R. Ulrich: J. Vac. Sci. Tech. **11**, 156 (1974)
43.45 P. K. Tien, A. A. Ballman: J. Vac. Sci. Tech. **12**, 892 (1974)
43.46 J. M. Mir, J. A. Agostinelli: J. Vac. Sci. Tech. A **12**, 1439 (1994)
43.47 J. Mueller, M. Mahnke, G. Schoer, S. Wiechmann: AIP Conference Proceedings **709**, 268 (2004)
43.48 D. Cangialosi, M. Wubbenhorst, H. Schut, A. van Veen, S. J. Picken: Phys. Rev. B **69**, 134206–1 (2004)
43.49 M. B. J. Diemeer: AIP Conference Proceedings **709**, 252 (2004)
43.50 N. Daldosso, M. Melchiorri, F. Riboli, F. Sbrana, L. Pavesi, G. Pucker, C. Kompocholis, M. Crivellari, P. Bellutti, A. Lui: Mat. Sci. Semicond. Proc. **7**, 453 (2004)
43.51 A. V. Kolobov (Ed.): *Photo-induced Metastability in Amorphous Semiconductors* (Wiley-VCH, Weinheim 2003)
43.52 K. Tanaka: C.R. Chimie **5**, 805 (2002)
43.53 H. Haeiwa, T. Naganawa, Y. Kokubun: IEEE Phot. Tech. Lett. **16**, 135 (2004)
43.54 K. Minoshima, A. M. Kowalevicz, E. P. Ippen, J. G. Fujimoto: Opt. Express **10**, 645 (2002)
43.55 N. Ponnampalam, R. G. DeCorby, H. T. Nguyen, P. K. Dwivedi, C. J. Haugen, J. N. McMullin, S. O. Kasap: Opt. Express **12**, 6270 (2004)
43.56 K. O. Hill: IEEE J. Sel. Top. Quant. Elec. **6**, 1186 (2000)
43.57 P. R. Herman, R. S. Marjoribanks, A. Oettl, K. Chen, I. Konovalov, S. Ness: Appl. Surf. Sci. **154–155**, 577 (2000)
43.58 M. Aslund, J. Canning: Opt. Lett. **25**, 692 (2000)
43.59 C. Florea, K. A. Winick: J. Light. Tech. **21**, 246 (2003)
43.60 A. Zakery, Y. Ruan, A. V. Rode, M. Samoc, B. Luther-Davies: J. Opt. Soc. Am. B. **20**, 1844 (2003)
43.61 X. Orignac, D. Barbier, X. Min Du, R. M. Almeida, O. McCarthy, E. Yeatman: Opt. Mat. **12**, 1 (1999)
43.62 R. A. Bellman, G. Bourdon, G. Alibert, A. Beguin, E. Guiot, L. B. Simpson, P. Lehuede, L. Guiziou, E. LeGuen: J. Electrochem. Soc. **151**, 541 (2004)
43.63 G.-L. Bona, R. Germann, B. J. Offrein: IBM J. Res. & Dev. **47**, 239 (2003)
43.64 A. J. Kenyon: Prog. Quant. Elec. **26**, 225 (2002)
43.65 M. J. Miniscalco: *Rare-Earth-Doped Fiber Lasers and Amplifiers*, 2nd edn. (Dekker, New York 2001), Chapt. 2
43.66 Y. Gao, B. Boulard, M. Couchaud, I. Vasilief, S. Guy, C. Duverger, B. Jacquier: Opt. Mat. **27**, 195–199 (2005)
43.67 T. Barwicz, M. A. Popovic, P. T. Rakich, M. R. Watts, H. A. Haus, E. P. Ippen, H. I. Smith: Opt. Express **12**, 1437 (2004)
43.68 T. Kawashima, K. Miura, T. Sato, S. Kawakami: Appl. Phys. Lett. **77**, 2613 (2000)
43.69 R. Rabady, I. Avrutsky: Appl. Opt. **44**, 378 (2005)
43.70 H. Hirota, M. Itoh, M. Oguma, Y. Hibino: IEEE Phot. Tech. Lett. **17**, 375 (2005)
43.71 C.-Y. Tai, J. S. Wilkinson, N. M. B. Perney, M. Caterina Netti, F. Cattaneo, C. E. Finlayson, J. J. Baumberg: Opt. Express **12**, 5110 (2004)

43.72 B. Unal, C.-Y. Tai, D. P. Shepherd, J. S. Wilkinson, N. M. B. Perney, M. Caterina Netti, G. J. Parker: Nd:Ta2O5 rib waveguide lasers, Appl. Phys. Lett. **86**, 021110 (2005)

43.73 Y. Kokubun, Y. Hatakeyama, M. Ogata, S. Suzuki, N. Zaizen: IEEE J. Sel. Top. Quant. Elec. **11**, 4 (2005)

43.74 T. Sato, K. Miura, N. Ishino, Y. Ohtera, T. Tamamura, S. Kawakami: Opt. Quant. Elec. **34**, 63 (2002)

43.75 D. R. MacFarlane: Ceramics International **22**, 535 (1996)

43.76 A. Feigel, M. Veinger, B. Sfez, A. Arsh, M. Klebanov, V. Lyubin: Appl. Phys. Lett. **83**, 4480 (2003)

43.77 G. Lenz, S. Spalter: *Nonlinear Photonic Crystals* (Springer, Berlin, Heidelberg 2003), Chapt. 11

43.78 K. Ogusu, J. Yamasaki, S. Maeda, M. Kitao, M. Minakata: Opt. Lett. **29**, 265 (2004)

43.79 S. Hocde, S. Jiang, X. Peng, N. Peyghambarian, T. Luo, M. Morrell: Opt. Mat. **25**, 149 (2004)

43.80 R. Nayak, V. Gupta, A. L. Dawar, K. Sreenivas: Thin Sol. Films **445**, 118 (2003)

43.81 D. Barbier: *Integrated Optical Circuits and Components, Design and Applications* (Dekker, New York 1999), Chapt. 5

43.82 B. E. Callicoatt, J. B. Schlager, R. K. Hickernell, R. P. Mirin, N. A. Sanford: IEEE Circuits & Devices Mag. **19**, 18 (September 2003)

43.83 E. DeSurvire: *Rare-Earth-Doped Fiber Lasers and Amplifiers, 2ed*. (Dekker, New York 2001), Chapt. 10

43.84 A. Yariv: *Optical Electronics in Modern Communications*, 5th edn. (Oxford Univ. Press, New York 1997)

43.85 Q. Wang, N. K. Dutta: J. Appl. Phys. **95**, 4025 (2004)

43.86 M. J. F. Digonnet: *Rare-Earth-Doped Fiber Lasers and Amplifiers*, 2nd edn. (Dekker, New York 2001), Chapt. 3

43.87 D. S. Funk, J. G. Eden: *Rare-Earth-Doped Fiber Lasers and Amplifiers*, 2nd edn. (Dekker, New York 2001), Chapt. 4

43.88 S. Saini, J. Michel, L. C. Kimerling: J. Light. Tech. **21**, 2368 (2003)

43.89 P. G. Kik, A. Polman: J. Appl. Phys. **93**, 5008 (2003)

43.90 P. Laporta, S. Taccheo, S. Longhi, O. Svelto, C. Svelto: Opt. Mat. **11**, 269 (1999)

43.91 F. J. Grawert, J. T. Gopinath, F. O. Ilday, H. M. Shen, E. P. Ippen, F. X. Kartner, S. Akiyama, J. Liu, K. Wada, L. C. Kimerling: Opt. Lett. **30**, 329 (2005)

43.92 U. Keller: Nature **424**, 831 (2003)

43.93 T. Qiu, L. Li, A. Schulzgen, V. L. Temyanko, T. Luo, S. Jiang, A. Mafey, J. V. Moloney, N. Peyghambarian: IEEE Phot. Tech. Lett. **16**, 2592 (2004)

43.94 Y. C. Yan, A. J. Faber, H. de Waal, P. G. Kik, A. Polman: Appl. Phys. Lett. **71**, 2922 (1997)

43.95 F. D. Patel, S. DiCarolis, P. Lum, S. Venkatesh, J. N. Miller: IEEE Phot. Tech. Lett. **16**, 2607 (2004)

43.96 A. Polman, F. C. J. M. van Veggel: J. Opt. Soc. Am. B **21**, 871 (2004)

43.97 H.-S. Han, S.-Y. Seo, J. H. Shin, N. Park: Appl. Phys. Lett. **81**, 3720 (2002)

43.98 J. Lee, J. H. Shin, N. Park: J. Light. Tech. **23**, 19 (2005)